IEEE Access
Multidisciplinary | Rapid Review | Open Access Journal

Received September 30, 2020, accepted November 28, 2020, date of publication December 22, 2020,
date of current version January 6, 2021.

Digital Object Identifier 10.1109/ACCESS.2020.3046668

Design and Implementation of a Fault-Tolerant Magnetic Bearing Control System Combined With a Novel Fault-Diagnosis of Actuators

XIN CHENG[1,2], SHUAI DENG[1], BAI-XIN CHENG[1], YE-FA HU[1,2], HUA-CHUN WU[1,2], AND ROU-GANG ZHOU[3], (Member, IEEE)

[1]School of Mechanical and Electronic Engineering, Wuhan University of Technology, Wuhan 430070, China
[2]Hubei Provincial Engineering Technology Research Center for Magnetic Suspension, Wuhan 430070, China
[3]School of Mechanical Engineering, Hangzhou Dianzi University, Hangzhou 310000, China

Corresponding author: Rou-Gang Zhou (zhourg@hdu.edu.cn)

This work was supported in part by the National Natural Science Funds of China under Grant 51205300 and Grant 51575411, in part by the National Key Research and Development Program of China under Grant 2018YFB2000103, and in part by the Fundamental Research Funds for the Central Universities under Grant WUT2017III046 and Grant 2020-YB-022.

ABSTRACT Although magnetic bearings are generally reliable, an important concern for machine applications is fault tolerance. The fault-tolerant operation of a magnetic bearing system can be realized through the identification and isolation of fault actuators and subsequent support reconstruction via residual actuators. In this study, a novel fault-diagnosis algorithm for electromagnetic actuators (EMAs) is proposed. The equivalent slope of the load current is defined as a fault-diagnosis threshold by theoretically analyzing the variation characteristics of the current in the modulation. The synchronous sampling of the current and its processing algorithm are designed. By combining these algorithms with the generalized bias current linearization theory reported previously, a fault-tolerant control (FTC) system for magnetic bearings is developed, and control of multi-position and multi-current loops is realized by using two digital signal processors (DSP). The FTC of the rotor motion and the fault-diagnosis of actuators are executed in parallel. The proposed control system is verified by the experiments, and experimental results demonstrate that the proposed system can cope with EMA fault in an extremely short time of less than 5 ms. Thus, the support can be reconstructed by employing the FTC to maintain rotor stability.

INDEX TERMS Control system design, fault tolerance, fault-diagnosis, magnetic bearing, parallel processing.

I. INTRODUCTION

The magnetic suspension support has certain specific properties, including the elimination of lubrication systems, low power loss due to the friction-free operation, and controllability of bearing dynamic characteristics. Typical applications of magnetic suspension support include the use of magnetically-levitated planar actuators [1]–[3] in degrees-of-freedom (DOF) ultra-precision stages and widespread use of magnetic bearings [4], [5] in rotating supporting parts. Magnetic bearings are a key component of aircraft engines, nuclear energy turbine generating plants, and energy storage flywheels [6]. Magnetic actuator failure, which is one of the major failures of conventional magnetic bearings with symmetric constraints on stator structures, can cause the rotor to fall out of control, resulting in serious damage to the whole bearing system [7].

Designed redundancy is an effective solution to this problem and can be realized in two ways. The first way to use the compensation strategy based on the loosely-coupled supporting structure, which is accomplished by direct force coupling between adjacent magnetic poles. The reconfiguration rules of this structure have been studied by Gu *et al.* [8]. The second way is to compensate the electromagnetic force (EMF) losses of faulted magnetic poles by using flux coupling, namely, to use a heteropolar [9] or the tightly-coupled redundant supporting structure [10]. As for the heteropolar supporting structure, Cheng *et al.* [11] proposed the generalized bias current linearization algorithm, which can continually maintain rotor bearings using the current redistribution when

The associate editor coordinating the review of this manuscript and approving it for publication was Jun Shen.

partial electromagnetic coil failure occurs. Following this theory, Maslen and Meeker [12] optimized the fault-tolerant control (FTC) scheme of electromagnetic actuators (EMAs) and presented an efficient optimization method based on the Lagrange multiplier approach. They also verified the effectiveness of the proposed method using flexible rotors [13], which ensured the displacement orbits of the rotors could be maintained before and after partial coil fault. Noh experimentally confirmed the theoretical feasibility of the generalized bias current linearization algorithm in vacuum molecular pumps equipped with magnetic bearings [14]. Noh *et al.* [15] proposed a generalized unbiased control strategy for radial magnetic bearings and extended the method of unbiased control for three-pole radial magnetic bearings to a generalized unbiased control strategy by encompassing bearings with an arbitrary number of poles. The principal objective for the FTC is to ensure the continual safe running of the rotor after the occurrence of a fault. It should be mentioned that structural redundancy of magnetic bearings facilitates activating the fault tolerance of a control system, and the fundamental theory of FTC has been established [7]–[15]. Nevertheless, the control system should be able to identify and isolate faulted actuators rapidly and accurately and then provide new support on the basis of the residual parts.

The fault detection methods for EMAs can be roughly divided into two categories. The first category includes the analytical and recognition technologies based on system models. For instance, for three-pole magnetic bearings, a linear relationship between the coil current and monitoring parameters was established and used to monitor and estimate system status [16]. In a five-DOF magnetic bearing system, a state-space equation based on modern control theory was established and used to detect, identify, and analyze faults [17]. In order to address the switch faults that commonly occur in power amplifier (PA) circuits, a detection strategy based on the instant voltage error in the converter, which can accurately identify faulted switches within two sampling periods in favorable conditions, was proposed in [18]. Moreover, the rotor motion equation of an eight-pole magnetic bearing scheme with biased discs was derived, and an identification algorithm based on the identification algorithm of least square regression was developed [19]. The system fault characteristics can be estimated online based on tiny rotor displacement (vibration) and current signals. The above-mentioned algorithms can decrease or eliminate the dependence on sensors during fault diagnosis, but the errors between mathematical models and real systems can further complicate fault recognition. In particular, there have not been any precise models targeting different fault signatures under different working conditions yet [20].

The second category includes fault detection methods based on the digital signal processing of sensor data. In these methods, the current and vibration signals can be obtained most easily, and these methods have been commonly used for the fault detection of stator, rotor, and bearings [21], [22]. The machine current signature analysis, which is a popular approach used in the fault-diagnosis of induction motors, employs current sensors to monitor the current and frequency-domain characteristics to detect differences between healthy and faulty conditions [23]. However, this approach fails to detect broken faults under a no-load condition because, in that case, the load current is comparatively small and unavailable for fault analysis. In order to overcome this problem, discrete wavelet analysis and higher-order spectra in an unloaded condition have been proposed [24], [25]. In addition, a modified bispectrum analysis based on the amplitude modulation feature of the current signal was adopted in [26] to combine lower and higher sidebands, and an effective diagnostic feature based on this bispectrum analysis was developed for fault classification. Moreover, a fault detection method based on the generalized likelihood ratio test was proposed, but its accuracy depended on the selection of a valid threshold [27]. By employing a bank of filters and defining the thresholds such that they explicitly account for the effect of uncertainty, a fault detection and isolation approach was proposed for diagnosing actuator and sensor faults in nonlinear uncertain systems [28]. Nevertheless, the fault detection methods in this category commonly suffer from two limitations:

1) The exact threshold cannot be identified by merely applying experience.
2) Complex digital signal processing sets strict requirements for processor performance, and this overhead in real-time systems may reduce system throughput to an unacceptable level.

In project magnetic bearings are applied to high-speed rotor systems and required to complete fault detection, isolation, and reconfiguration in a real-time environment. Therefore, in the event of failure, the control system can rapidly provide efficient support before the rotor falls and maintain rotor stability during support reconfiguration. A real-time, threshold-based fault detection algorithm without a valid threshold was put forward in [10], but the diagnostic results were less accurate when the control currents of the actuator changed suddenly. Given that the ripple characteristics of the actuator current are directly correlated with the time constant of electromagnetic coils [29], theoretical analysis and simulation validation of the inherent ripple characteristics have been conducted in [30], [31].

Motivated by the related work presented above, this paper proposes a fault-tolerant magnetic bearing control system (MBCS) implementation scheme based on two digital signal processors (DSPs) and designs relevant block diagrams of software and hardware.

The main contributions of this paper can be summarized as follows.

1) A novel real-time electromagnetic coil fault detection algorithm for EMAs is proposed, and an equivalent slope of the load current within the modulation period is defined and preset as a valid threshold of fault detection.

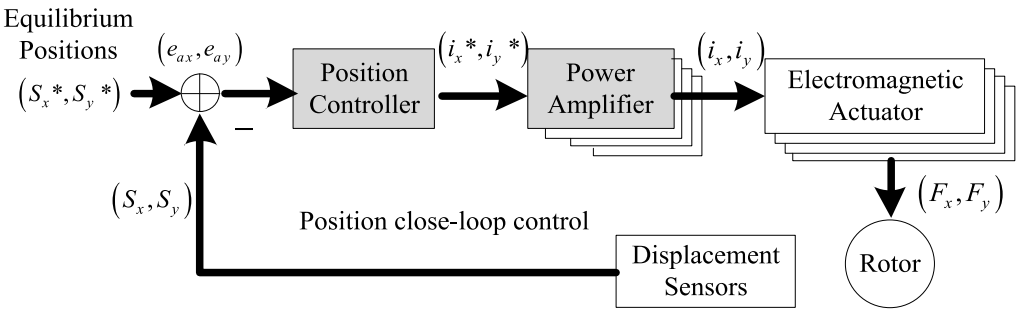

FIGURE 1. Conventional MBCS.

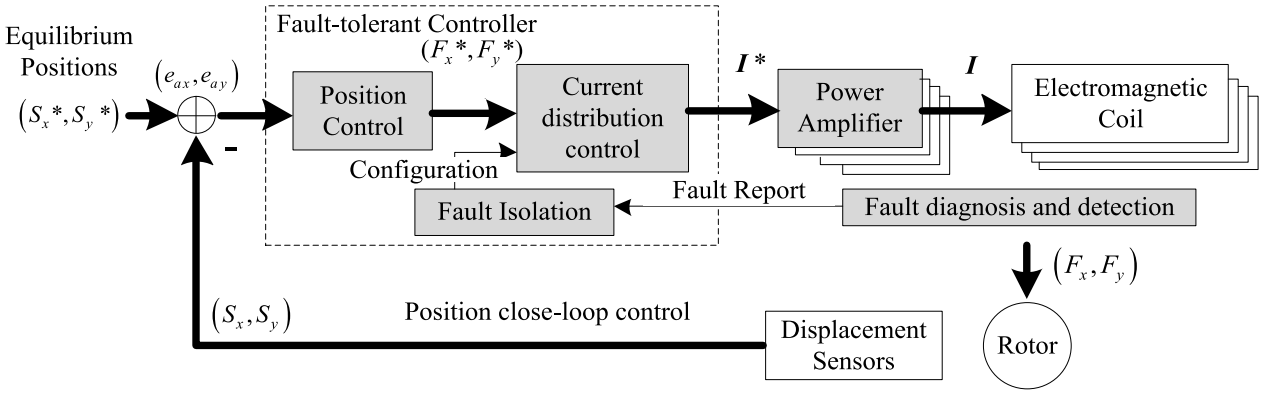

FIGURE 2. Configuration of the FTC system for magnetic bearing with a redundant structure.

2) A fault-tolerant MBCS combined with the proposed fault detection algorithm is designed and realized. The complex control algorithms with heavy computation are developed by software using two DSPs, and the FTC of the rotor motion and fault diagnosis of actuators are executed in parallel.

The rest of the paper is structured as follows. Section II briefly describes the control system requirements and configuration. Section III presents the design and implementation of the proposed control system, including the novel fault diagnosis and detection method, and the detailed implementation of the FTC system. Section IV details the experimental results and analysis. Finally, Section V draws the conclusions and presents future work directions.

II. SYSTEM REQUIREMENTS AND CONFIGURATION

The block diagram of the MBCS with radial magnetic bearings is shown in Fig. 1. The position controller produces control currents $\left(i_x^*, i_y^*\right)$ according to the position comparator outputs, and position error e is easily computed by $e_i(k) = S_i(k)^* - S_i(k)$. The closed-loop current control is usually accomplished in PAs by generating currents $\left(i_x, i_y\right)$, which form the designed EMFs$\left(F_x, F_y\right)$ according to the control currents.

Usually, each electromagnetic coil and the corresponding PA constitute a channel of a multi-current closed loop. Faults in a channel (e.g., broken circuit, short circuit, or magnetic pole damage) can cause an actuator failure, meaning actuators cannot produce the designed EMF. In the case of a symmetrical eight-pole radial magnetic bearing, when a certain pole or multiple poles fail, the pole flux can be compensated by the control current redistribution owing to pole coupling [10], [11]. The configuration of an MBCS with a fault-tolerant controller is displayed in Fig. 2. Thus, the system requirements are listed as follows.

1) The overall EMA operation is monitored by the fault-diagnosis and detection (FDD) module, so the system can rapidly detect, diagnose, and isolate faulty actuators.
2) The current distribution control cell implements the current distribution strategy according to the actuator status and designed EMFs $\left(F_x^*, F_y^*\right)$. As a result, this cell creates the desired control current $\boldsymbol{I}^*$ in the form of a PWM to drive the power bridges in PAs.
3) The FTC system is constructed such that it enables parallel data processing, which can improve the overall real-time system performance. Once a fault occurs, the support of the magnetic bearing can be restored to a valid level before the falling of the rotor. In addition, the system maintains rotor stability during support reconfiguration.

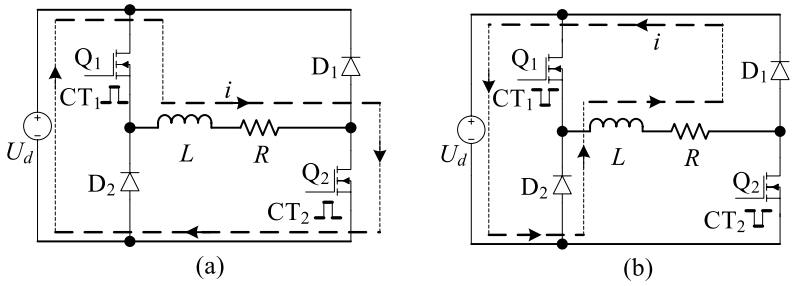

FIGURE 3. Current flows under the bi-state modulation. (a) Current-increasing process. (b) Current-decreasing process.

III. DESIGN AND IMPLEMENTATION OF FAULT-TOLERANT CONTROL SYSTEM

A. MATHEMATIC PRINCIPLE OF FAULT-DIAGNOSIS AND DETECTION

The principle of a bi-state unidirectional digital switch PA is illustrated in Fig. 3, where CT_1 and CT_2 denote the driving signals of switching tubes Q_1 and Q_2 on the power bridge, respectively, with the duty cycle employed to control the change in the coil current. When Q_1 and Q_2 are enabled simultaneously, the coil current rises, as shown in Fig. 3(a). However, when Q_1 and Q_2 are disabled simultaneously, the coil, through the freewheeling diodes D_1 and D_2, forms a closed circuit with the power source, and the coil current decreases, as shown in Fig. 3(b), where U_d denotes the power bus voltage, and L and R denote the equivalent inductance and resistance of the coil, respectively. The coil current can be controlled by the power tube drive signals CT_1 and CT_2 from a configurable PWM generator.

When the load current increases, we have:

$$U_d = L\frac{\mathrm{d}i(t)}{\mathrm{d}t} + Ri(t) + 2U_s, \tag{1}$$

where U_s denotes the conduction voltage drop of the switch tube, and i represents the load current of the magnetic coil.

By solving equation (1), we obtain:

$$i(t) = \frac{U_d - 2U_s}{R}(1 - \mathrm{e}^{-\frac{t}{\tau}}) + i_0\mathrm{e}^{-\frac{t}{\tau}}. \tag{2}$$

By taking the derivative of current, the slope of the load current can be obtained by:

$$k_{inc} = \frac{\mathrm{d}i(t)}{\mathrm{d}t} = \frac{U_d - 2U_s}{L}\mathrm{e}^{-\frac{t}{\tau}} - \frac{i_0}{\tau}\mathrm{e}^{-\frac{t}{\tau}}. \tag{3}$$

Similarly, the slope of the load current when the load current decreases can be determined as:

$$k_{dec} = \frac{\mathrm{d}i(t)}{\mathrm{d}t} = -\frac{U_d + 2U_c}{L}\mathrm{e}^{-\frac{t}{\tau}} - \frac{i_0}{\tau}\mathrm{e}^{-\frac{t}{\tau}}. \tag{4}$$

As shown in Fig. 4, the current slope in the current-increasing process should satisfy the following conditions:

$$\begin{cases} k_{\max} = \dfrac{U_d - 2U_s}{L} - \dfrac{i_0}{\tau} \\ k_{\min} = \dfrac{U_d - 2U_s}{L} \cdot \mathrm{e}^{-(\frac{T}{2})/\tau} - \dfrac{i_0}{\tau} \cdot \mathrm{e}^{-(\frac{T}{2})/\tau} \end{cases}, \tag{5}$$

where i_0 denotes the initial current of the magnetic coil, and $\tau = L/R$ denotes the time constant of the magnetic coil.

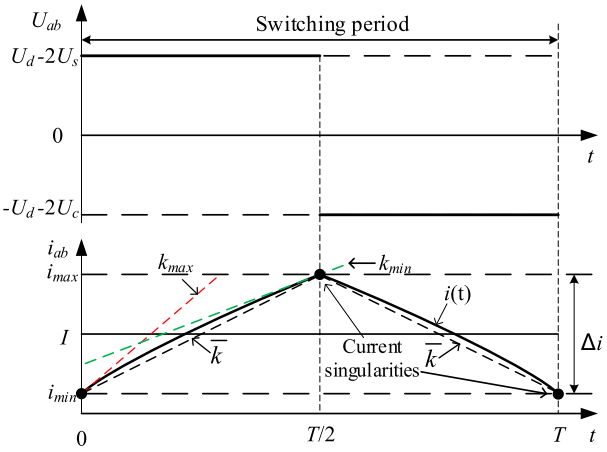

FIGURE 4. The slopes of the load current in the switching period [31].

Since τ is far larger than the switch cycle T of the PA, $\mathrm{e}^{-t/\tau} \approx 1$ and the slope of load current is approximately linear, which is expressed as:

$$k_{\min} \approx k_{\max} \approx k_{inc} = \frac{U_d - 2U_s - i_0R}{L} = \bar{k}. \tag{6}$$

The equivalent resistance R of a coil is usually at the level of mΩ, and the effect of i_0R on the load current slope is negligible relative to the power bus voltage U_d. Obviously, the slope of the load current within a PMW modulation period is an inherent physical property of the coil and independent of the current control algorithm. Moreover, the slope is slightly affected by the load current value. As a result, the equivalent slope of the load current can be defined, and therefore, the theoretical range can be set. Once a coil failure occurs (e.g., broken circuit, short circuit, or even partial insulation damage), the equivalent slope of the load current will deviate from the preset range.

B. DESIGN OF MULTI-CHANNEL POWER AMPLIFIER WITH FAULT-DIAGNOSIS AND DETECTION

The PA, including a current controller, FDD module, and power stage, is designed, and it is presented in Fig. 5. The power stage consists of an H-type power bridge, a gate driver, a current sensor, and a low-pass filter (LPF). The power stage enables power devices according to the PWM signals for the

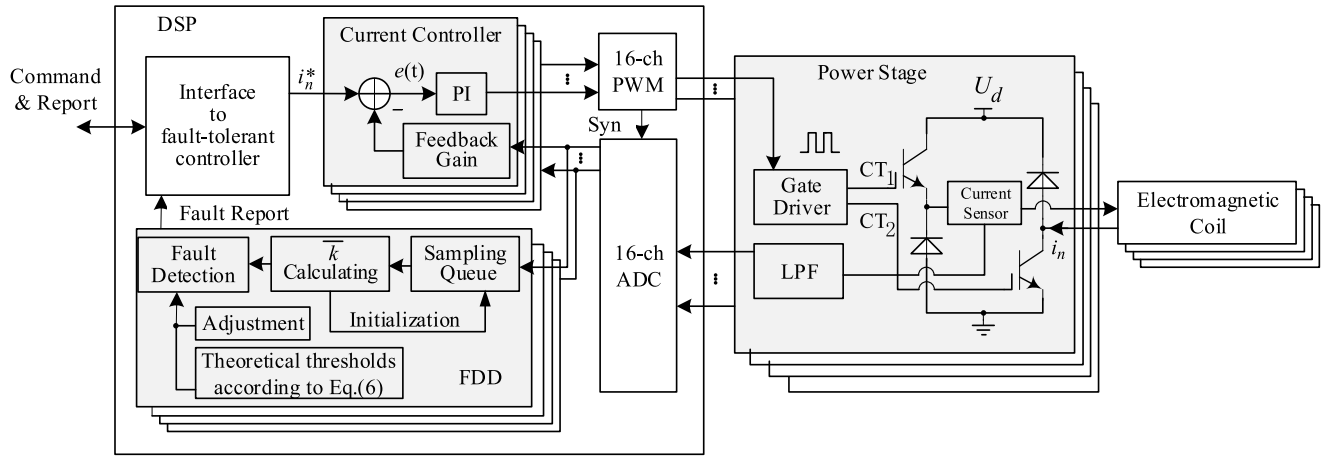

FIGURE 5. Multi-channel PA with the FDD module.

sake of controlling the load current. In addition, the current controller adopts the PI algorithm to decrease the error $e(t)$ between the designed current i_n* and the load current i_n, and the closed-loop negative feedback control is constructed by transmitting the current value to the current controller through a 16-channel ADC, whereas the PA output is used as a preset. The presented design has two innovations. First, a multi-channel PA, which should be realized in a decentralized mode, can be simply achieved by combining a DSP with multiple power stages, and the current controller and feedback gain can be implemented by software. Second, each current control closed loop corresponds to an independent FDD module, and the current sampling is discretized into a sampling point queue, which is used by the FTC system to estimate the status of actuators by calculating the equivalent slope of the load current. In this way, the unified fault-description for multi-channel PA is realized after fault detection. The design of the FDD module is introduced in the following.

In software realization, two factors need to be considered during the design process of an FDD module. First, the FTC system effectively increases the number of configurable EMAs under fault conditions, but the operation status of all of the EMAs must be described with a general index. The description of this index will be introduced in Section III-C. Second, the broken or short circuit of the closed-loop current control can be easily judged because the coil currents under such faults are uncontrolled. Moreover, this situation, in which the load current of a normal coil is close to zero during the rotor motion control, should be taken into account to improve the functionality of the FTC system. In some situations, such as partial insulation failure of electromagnetic coils, the coil currents can be controlled. However, since the numbers of winding turns, flux, and magnetic circuit characteristics are changeable, the dynamic properties of EMAs will deviate significantly, thus demanding from the fault-diagnosis module to respond to the above situations rapidly.

The working procedure of the proposed FDD includes sequential sampling of the current data, rapid calculation of $\bar{k}$, and fault detection. The PWM module enables the ADC module directly through a synchronization signal, as shown in Fig. 6(a), which further guarantees the phase feature of the current sampling sequence within a modulation period, as shown in Fig. 6(b). At time t_2, whose delay time in the power-down control is T_{de} compared to the first sampling time t_1, the sampling data a_1 are stored in the first-in-first-out (FIFO) manner. In addition, the processing speed of the system can be greatly improved by utilizing the design, in which the CPU accesses data via DMA (direct memory access) bus. Similarly, the sampling data during the subsequent intervals $t_3 - t_9$ are stored in the same way until time t_{10}. Then, the next synchronization signal is acquired to activate a new round of sequential sampling.

In order to improve the real-time performance and precision of calculating the equivalent slope of the load current, the segmental calculation and data sampling are performed in a pipelined way. From two adjacent current sampling points shown in Fig. 6(b), we have:

$$k_i = G_f G_{LPF} \frac{(a_{i+1} - a_i) \cdot U_{REF}}{2^n T}, i = 1, 2, \ldots, \qquad (7)$$

where G_f denotes the feedback gain, G_{LPF} denotes the steady-state gain of the LPF, T denotes the sampling period of the ADC, U_{REF} denotes the built-in reference voltage of the ADC, and n denotes the ADC resolution. According to the current variation between two adjacent points, which is shown in Fig. 7, the equivalent slope of the load current in the current-rising process is expressed as follows:

$$\bar{k}_{inc} = \frac{k_1 + \cdots + k_{i-3} + k_{i-2} + k_{i-1} + k_i}{i}. \qquad (8)$$

Furthermore, the singularities that belong to the sampling points and are likely to be an error factor in the calculation of $\bar{k}_{inc}$ must be taken into consideration. An effective identification strategy to cancel these singularities has been presented in [31].

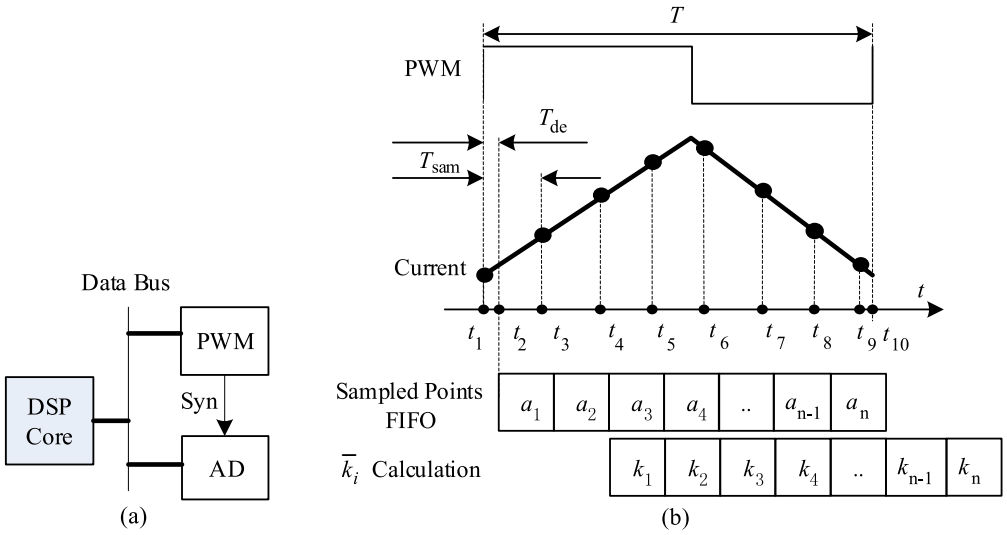

FIGURE 6. Sequential sampling and synchronization design in the modulation period.

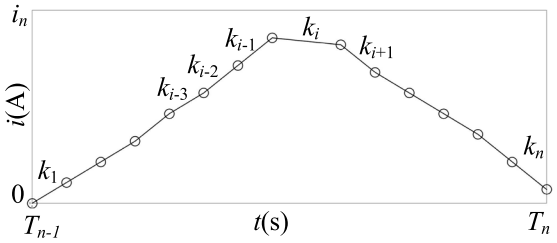

FIGURE 7. The slope of current variation between two adjacent sampling points [31].

C. IMPLEMENTATION OF FAULT-TOLERANT CONTROL SYSTEM

The typical mathematical model of a heteropolar radial magnetic bearing with a redundant supporting structure in a two-axis $x - y$ reference frame can be expressed as follows [11]:

$$\begin{cases} F_x = \boldsymbol{B}^{\mathrm{T}}\boldsymbol{D}_x\boldsymbol{B} \\ F_y = \boldsymbol{B}^{\mathrm{T}}\boldsymbol{D}_y\boldsymbol{B} \\ \boldsymbol{D}_x = \dfrac{A}{2\mu_0} diag\left[\cos\theta_1 \ \cos\theta_2 \ \cdots \cos\theta_n\right] \\ \boldsymbol{D}_y = \dfrac{A}{2\mu_0} diag\left[\sin\theta_1 \ \sin\theta_2 \ \cdots \sin\theta_n\right] \end{cases}, \tag{9}$$

where F_j denotes the resultant EMF from magnetic poles, A denotes the pole face area, μ_0 denotes the vacuum permeability, matrices $\boldsymbol{D}_j$ and $\boldsymbol{B}$ denote the structural parameters of the magnetic bearing and the flux density vector, respectively, and they can be expressed as [10], [11], [14]:

$$\boldsymbol{B} = \boldsymbol{R}^{-1}\boldsymbol{N}\boldsymbol{I}\boldsymbol{A}^{-1}, \tag{10}$$

where $\boldsymbol{R}$, $\boldsymbol{N}$, and $\boldsymbol{I}$ denote the reluctance matrix, coil winding influence matrix, and coil current vector, respectively. Based on equations (9) and (10), even when a certain coil fails and the corresponding magnetic field energy is zero, the above processes are not affected, and equation (9) still applies. In other words, the lost pole flux can be compensated by the current redistribution, which generates the designed EMFs. We define:

$$\boldsymbol{V} = \boldsymbol{A}^{-1}\boldsymbol{R}^{-1}\boldsymbol{N}. \tag{11}$$

Then, equation (9) can be transformed into:

$$\begin{cases} F_x = \boldsymbol{I}^{\mathrm{T}}\boldsymbol{V}^{\mathrm{T}}\boldsymbol{D}_x\boldsymbol{V}\boldsymbol{I} \\ F_y = \boldsymbol{I}^{\mathrm{T}}\boldsymbol{V}^{\mathrm{T}}\boldsymbol{D}_y\boldsymbol{V}\boldsymbol{I} \end{cases}. \tag{12}$$

The relationship between the current vector $\boldsymbol{I}$(when a fault occurs, it is a reduced order vector) and the produced forces F_j is quadratic. In order to realize the control model using software, the current distribution matrix $\boldsymbol{W}$ that satisfies equation (13) is defined as follows [11]:

$$\begin{cases} \boldsymbol{W}^{\mathrm{T}}\boldsymbol{V}^{\mathrm{T}}\boldsymbol{D}_x\boldsymbol{V}\boldsymbol{W} = \boldsymbol{M}_x \\ \boldsymbol{W}^{\mathrm{T}}\boldsymbol{V}^{\mathrm{T}}\boldsymbol{D}_y\boldsymbol{V}\boldsymbol{W} = \boldsymbol{M}_y \\ \boldsymbol{M}_x = \begin{bmatrix} 0 & 1/2 & 0 \\ 1/2 & 0 & 0 \\ 0 & 0 & 0 \end{bmatrix} \\ \boldsymbol{M}_y = \begin{bmatrix} 0 & 0 & 1/2 \\ 0 & 0 & 0 \\ 1/2 & 0 & 0 \end{bmatrix} \end{cases} \tag{13}$$

The coil current can be computed by $\boldsymbol{I} = \boldsymbol{W}\boldsymbol{I}_c$, where:

$$\boldsymbol{I}_C = \begin{bmatrix} C_0 & i_x & i_y \end{bmatrix}^{\mathrm{T}}, \tag{14}$$

and where C_0 denotes the bias current coefficient, and i_x and i_y are the control currents in the $x-$ and $y-$ directions, respectively. Then, equation (12) can be simplified to:

$$\begin{cases} F_x = C_0 i_x \\ F_y = C_0 i_y \end{cases}. \tag{15}$$

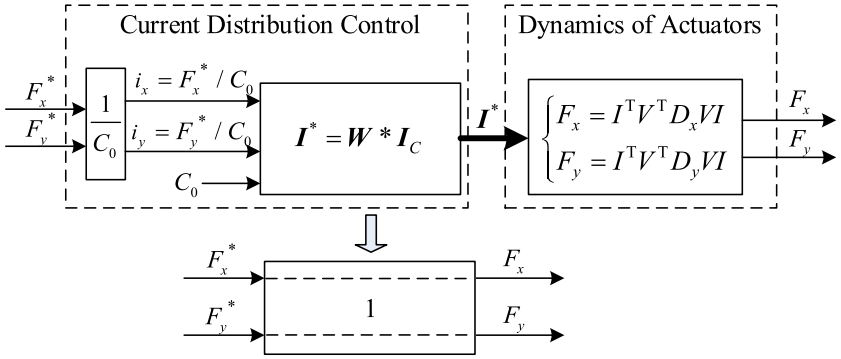

FIGURE 8. Block diagram of the current distribution control.

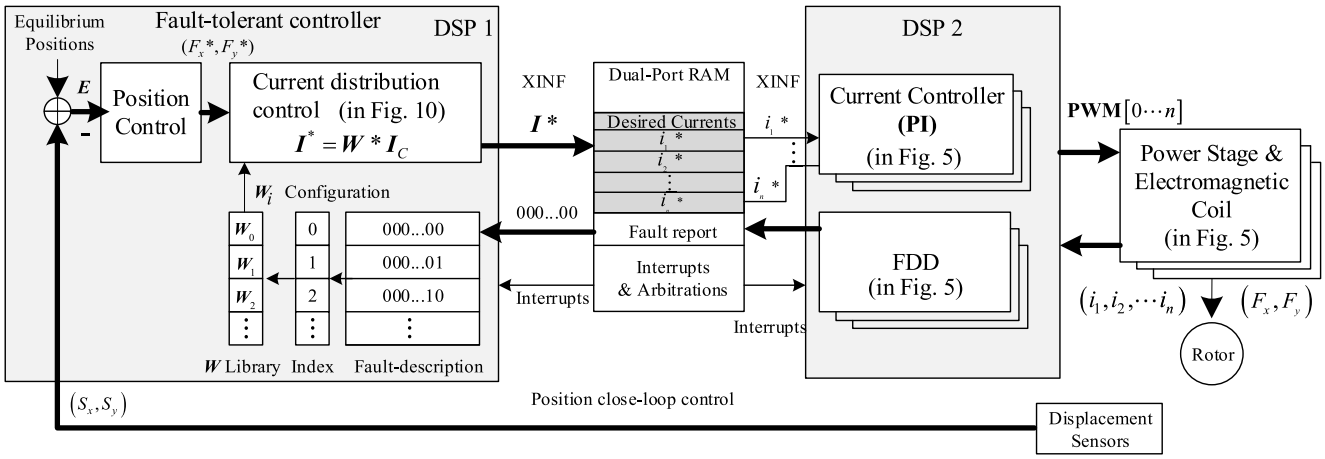

FIGURE 9. Design of a dual-DSP-based FTC system.

The fault tolerance of MBCS means that the system can establish a decoupling and linearized current–EMF relationship according to the existing dynamics of the EMAs. Regardless of a fault occurs or not, the designed EMFs can be realized using the current distribution control model. If the model is inverse to the real-time actuator dynamic model shown in Fig. 16(a), the EMFs shown in Fig. 8 can be realized. The above analyses imply that the FTC system under any fault state can determine a current distribution matrix $\boldsymbol{W}$ that matches with the actuator dynamics under the real-time condition. Thereby, the system can realize support reconfiguration, thus making $[F_x*, F_y*] = [F_x, F_y]$.

The FTC system based on two DSPs and a dual port random access memory (DPRAM) as a channel of data interaction is illustrated in Fig. 9. The interaction data of the control system consists of the following information: (1) the desired control current commands sent from the upper CPU to the current controller; (2) the fault report describing the fault states of actuators, which is sent from the lower FDD module to the upper CPU; and (3) interruption and arbitration data used to create bidirectional interruption information.

When the fault states are updated, the interruption to DSP 1 is valid, and a new matrix $\boldsymbol{W}$ is initiated. The interruption to DSP 2 is valid when the data of the closed-loop current control are updated, and it is used to notify the current controller to update the control command. These mechanisms ensure data consistency during synchronous reading and writing by DPRAM [5].

The FTC is realized by DSP 1 and belongs to the upper part of the whole control system, including a position controller and a current distribution control block. In this article, the PID algorithm is employed to eliminate rotor position errors. The configuration process of the current distribution matrix is presented in Fig. 9, where it can be seen that the fault report data (Fig. 5) that activate the current distribution control block are updated when the lower CPU detects a newly-formed fault of EMAs. According to this information, which forms a fault index, the faulted actuators are isolated by the current distribution control block. The fault index is used in $\boldsymbol{W}$ library to select $\boldsymbol{W}_i$, which is updated in the current distribution control cell according to the real-time fault-description.

The closed-loop current control and FDD modules are realized by DSP 2. By using the PI algorithm, PWM signals are obtained to control the power devices at the power stage to initiate the duty ratio and make $\boldsymbol{I}* = \boldsymbol{I}$. More details of sequential sampling and synchronization design can be found in Fig. 6. Meanwhile, each current control closed loop

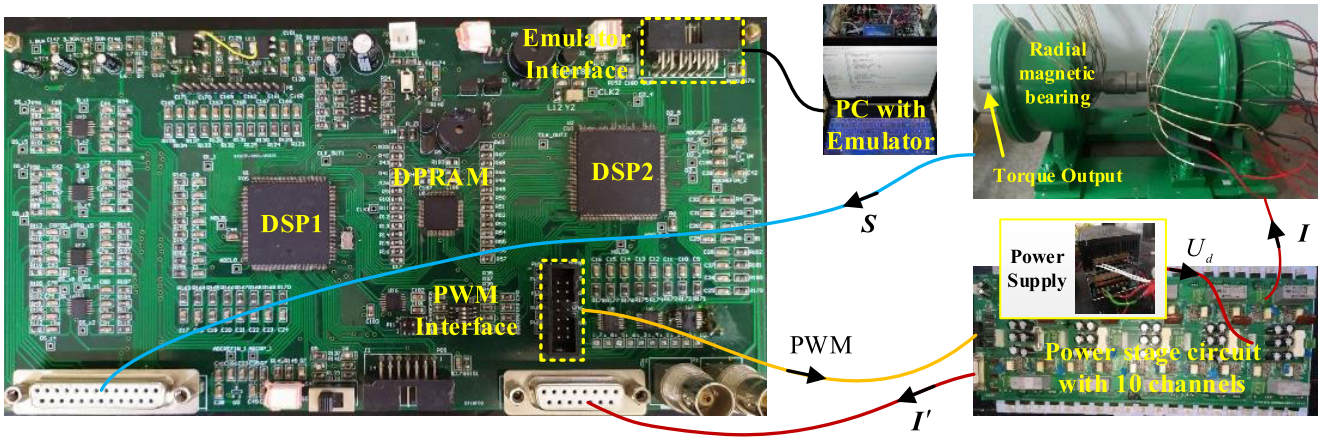

FIGURE 10. Experimental platform. I represents the load current, I' represents the feedback current, and S represents the rotor position.

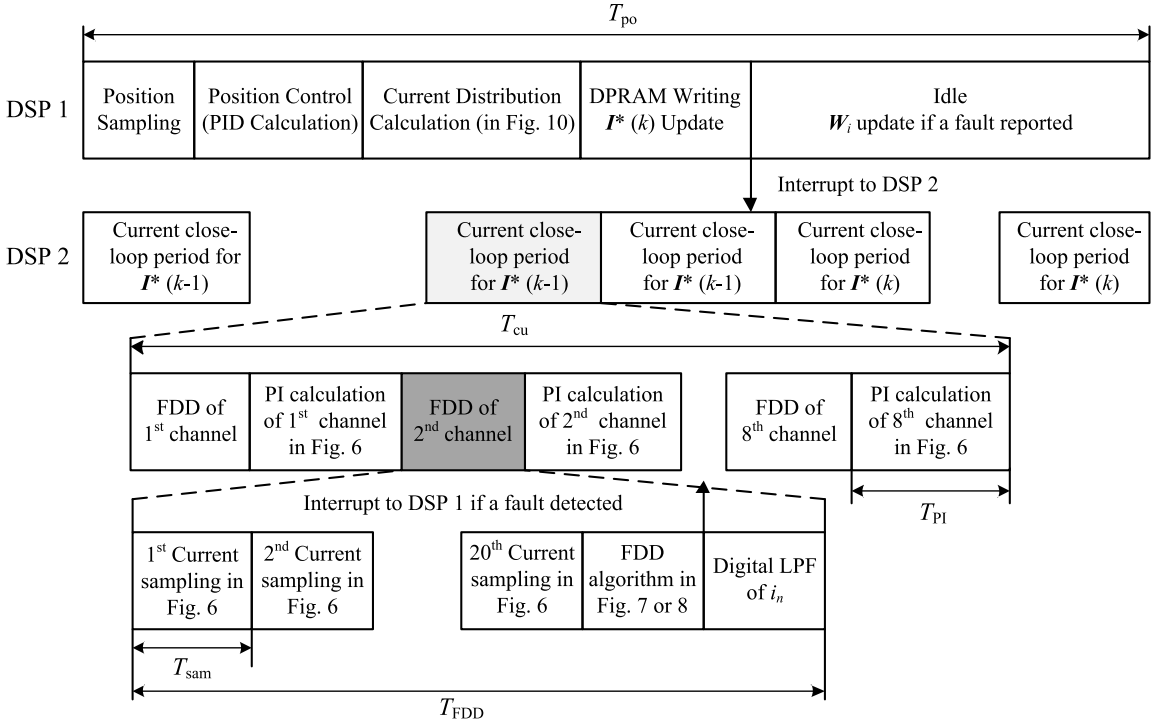

FIGURE 11. The timing sequences of the modules in the FTC system.

corresponds to one FDD module, aiming to estimate the inherent current ripple characteristics and compare them with the theoretical threshold. If a fault of a closed loop is detected, the fault information "1" is output by the software and the operational information on all of the closed loops is stored in the fault-report register. For instance, 000…010 means the fault corresponds to the second channel of the current control closed loops, so this channel is isolated subsequently.

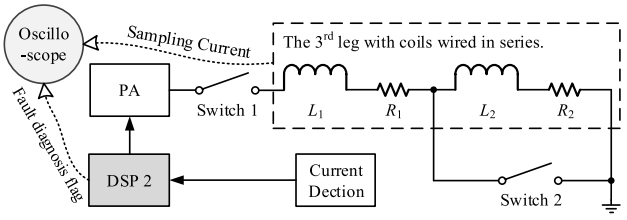

FIGURE 12. Load in the experiment: $L_1 \approx 1.76$mH, $R_1 \approx 0.48\,\Omega$, $L_2 \approx 1.50$mH, and $R_2 \approx 0.41\,\Omega$.

IV. EXPERIMENTAL RESULTS ANALYSIS

A. EXPERIMENTAL SETUP

The fabricated FTC system for a magnetically-levitated rotor with a redundant support structure is shown in Fig. 10. This system was implemented in software by using two TMS320F28335 DSPs working at the 150 MHz clock cycle rate and having IDT71V30 as a DPRAM; the reading and

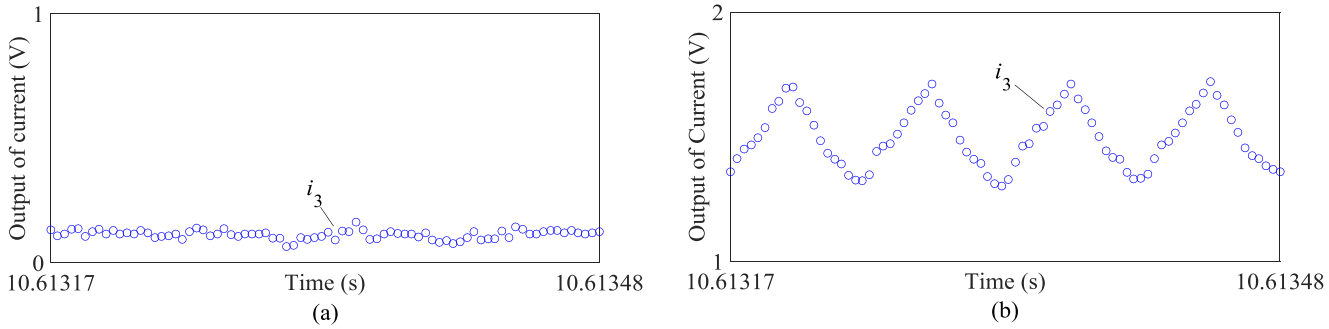

FIGURE 13. Sampling points of the load current at the fault stage. (a) Under a broken circuit fault. (b) Under a partial short circuit fault.

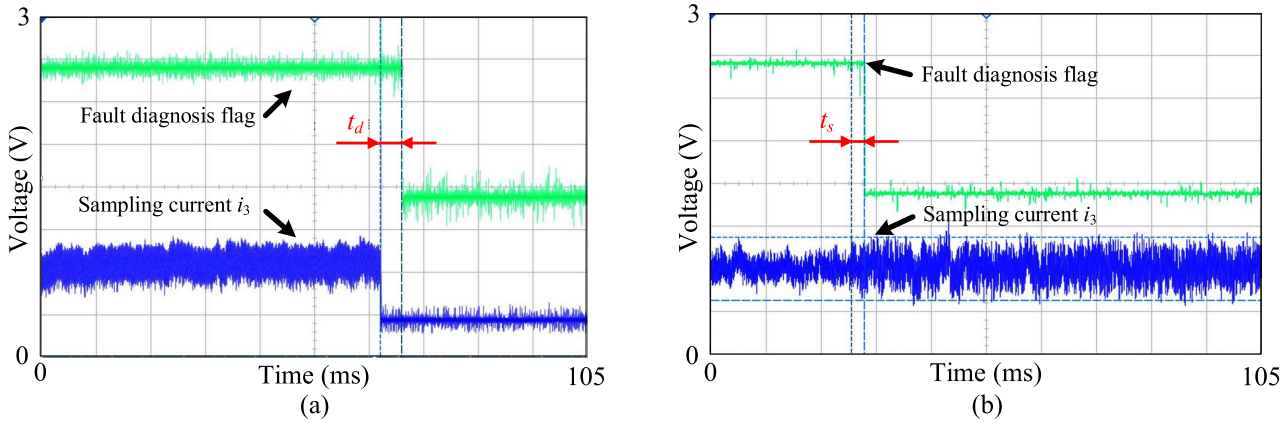

FIGURE 14. The fault-diagnosis time. (a) t_d under a broken circuit fault. (b) t_s under a partial short circuit fault.

writing speeds of interaction data were 10^9 Hz. One channel of the power stage circuit contained an IRFB4020Pb MOSFET, and a CSNE151-100 Honeywell current sensor was used as a conditioning circuit. The main structural parameters of the magnetic bearing are given in TABLE 1.

TABLE 1. Parameters of magnetic bearing.

Symbol	Description	Value	Unit
A_j	Pole area	$1.8{\cdot}10^{-3}$	m^2
N_j	Number of turns per coil	120	/
g_j	Air gap length	$5{\cdot}10^{-4}$	m
θ_j	Pole angle	$(j\text{-}1){\cdot}\pi/4$	rad

As a CPU for the lower control part (Fig. 9), DSP 2 constituted the multi-channel PA, including an FDD module and the power stage circuit. Considering the dynamic bandwidth of PA, the pulse period of the PWM generator in DSP 2 was set to 83.3 μs at 12 kHz. Following the sequential sampling and synchronization design presented in Section III-B, the A/D converting clock frequency was the same as the frequency of the PWM wave used to drive MOSFET. Hence, the A/D sampling period T_{sam} of DSP 2 was 4.2 μs at 240 kHz. On this basis, the sampling rate of the rotor position signals was 833 μs at 1.2 kHz. The current controller parameters were $P = 40$ and $I = 30$. To prevent numerical overflow, the output values of the PID/PI controller were both limited to a specific range. Moreover, a power filter was designed to maintain the stability of the bus voltage and prevent switching noise from being transmitted to the power supply. In the performance tests of the FTC system, which is presented in Section IV-B, the rotor speed was set to 3000 rpm, the sampling rate of the rotor position signals on the data acquisition card was 800 Hz, and the operating frequency of the oscilloscope was 240 kHz.

The time sequences of different modules in the FTC system are presented in Fig. 11. The position control loops and the current control loops were executed inside different DSPs to enhance system performance by parallel processing; namely, when the position loop calculation in DSP 1 ended, a new current distribution command was obtained according to the real-time $\boldsymbol{W}_i$ and written into the DPRAM after the external interruption instruction notified DSP 2. Then, the multiple current control modules in DSP 2 and the corresponding FDD modules operated in series. When a fault occurred, the actuator state in DPRAM was updated after the external interruption instruction notified DSP 1. The overheads of the critical modules are shown in TABLE 2, and these

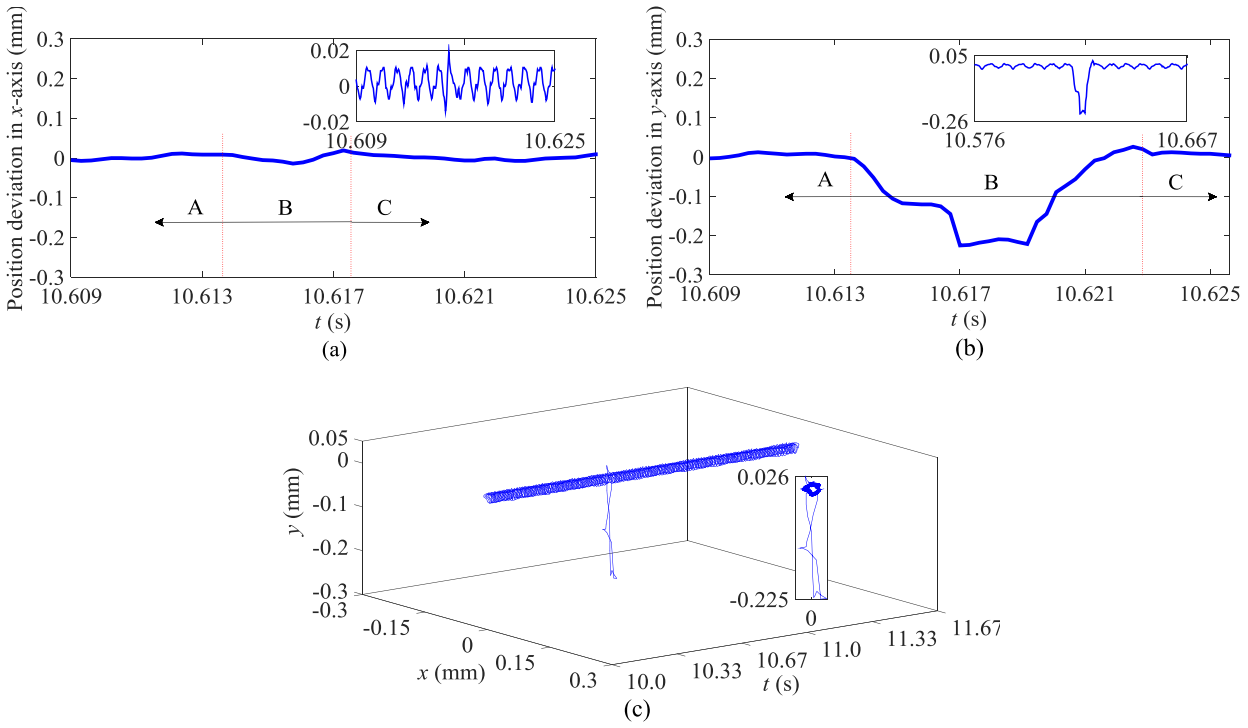

(a) normal stage, (b) fault stage, (c) fault tolerant stage.

FIGURE 15. Trajectory tracking of the rotor's torque-output end under a broken circuit fault. (a),(b) Rotor position deviation. (c) Rotor trajectory.

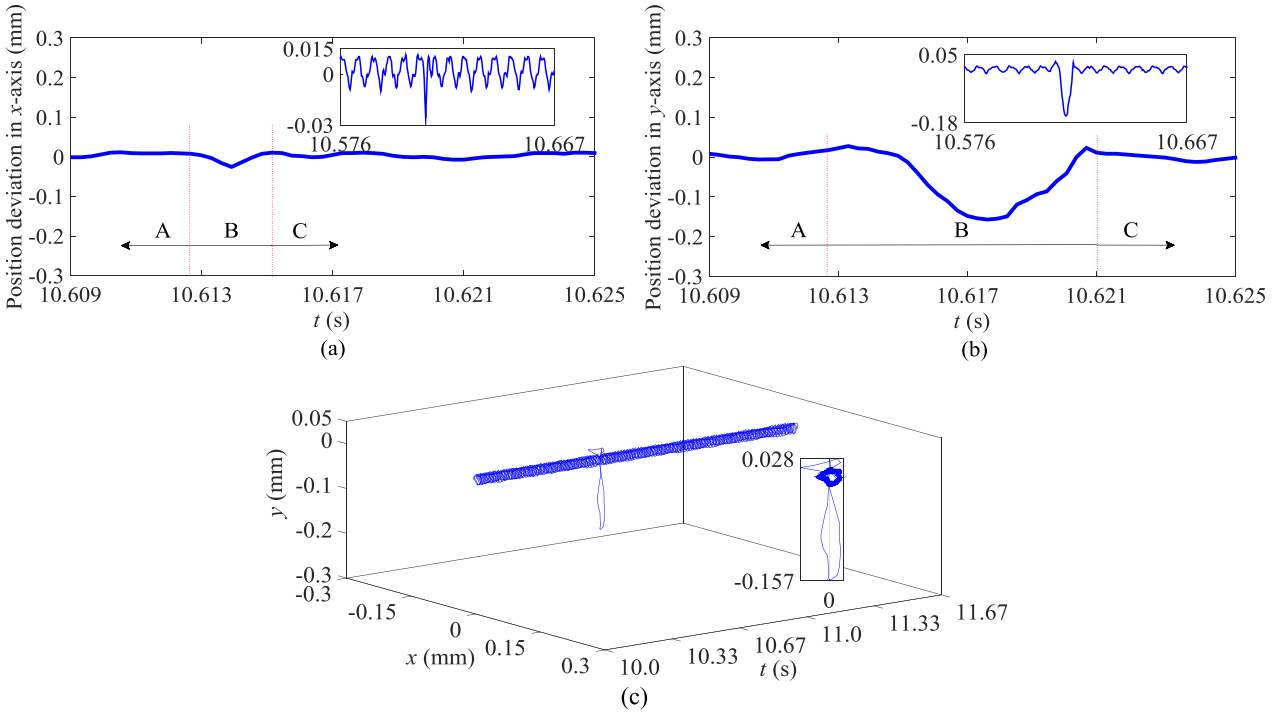

(a) normal stage, (b) fault stage, (c) fault tolerant stage.

FIGURE 16. Trajectory tracking of the rotor's torque-output end under a partial short circuit fault. (a),(b) Rotor position deviation. (c) Rotor trajectory.

values were measured by the CCS Profile clock when the proposed algorithm was running in the DSP with the core clock of 150 MHz.

B. EXPERIMENTAL RESULTS

The effectiveness of the FDD module for EMAs and the performance of the rotor motion control were evaluated under

TABLE 2. Overhead of the critical modules.

Parameter	T_{po}	T_{cu}	T_{pi}	T_{sam}	T_{FDD}
Value (μs)	6664.0	829.6	4.8	4.2	103.1

fault conditions on the magnetically-levitated rotor platform. In the experiment, the faults of coils were used to test the effectiveness and real-time performance of the FDD module. It should be noted that any failure in the power stages and the electromagnetic coils, which led to the change in the equivalent slope of the load current, would enable the FDD module according to the proposed fault detection algorithm.

First, a magnetic bearing, whose third leg had coils wired in series, was designed for the rotor's torque-output end (Fig. 10) to verify the performance of the FDD module. Following the circuit structure displayed in Fig. 12, the broken circuit or partial short circuit faults were realized by opening switch 1 or closing switch 2. In this work, the initial constants of the coil were 3.3 mH and 0.9 Ω, the bus voltage U_d was 45 V, and i_0 was 0.5 A; thus, according to equation (6), the theoretical range of the slope of the load current was [13626, 13646] according to equation (6).

When the third channel of the EMAs failed, the load current characteristics of this channel within four cycles were analyzed by MATLAB, and the discrete points are shown in Fig. 13. During the current-increasing process, after the broken circuit or partial short circuit fault occurred, the equivalent slope of i_3 was $[1121, 2831]$ or [25466, 25670], respectively. The fault signal was flagged according to the fault-diagnosis algorithm. Meanwhile, the pin output of DSP 2 and the coil load current were monitored by an oscilloscope, and the results are shown in Fig. 14. As shown in Fig. 14, the alarm signal from the lower CPU decreased from a high to a low level, and the time for fault diagnosis was about 5 ms.

Next, the motion trajectory control was used to evaluate the dynamic performance of the proposed FTC system under the condition of actuator failure. The trajectory tracking of the rotor's torque-output end is shown in Figs. 15 and 16. Relative to the gap of 0.300 mm between the magnetic bearing and the back bearing, the maximum rotor position deviation was 0.244 mm, indicating that the architecture of parallel processing of rotor motion FTC and the fault-diagnosis of EMA denoted an effective solution for improving the reliability of the magnetic bearing systems. Under the timing sequence shown in Fig. 11, and under fault conditions, the MBCS could reconstruct rotor support within 10 ms and prevent the rotor from falling.

V. CONCLUSION

In order to improve the fault tolerance in active magnetic bearing equipped machinery, an FTC system for magnetic bearings based on a real-time fault-diagnosis algorithm for EMAs is successfully realized using two DSPs. The stable suspension of the rotor under fault condition represents a software-related task and can be easily realized without any additional hardware. The computational cost of critical modules is measured running on line, which reveals that the proposed control strategies are streamlined. The broken circuit and partial short circuit faults can be detected for about 5 ms by the FDD module. The dynamic performance of the proposed MBCS under the condition of actuator failure is evaluated by the rotor motion trajectory, which reveals that the MBCS can reconstruct rotor support in 10 ms and thus prevents the rotor from falling. The experimental results show that the proposed system can provide fault detection and isolation for EMA, as well as a reconfiguration of the coil driving, to enable the continued safe running of the rotor during the occurrence of a fault.

Future work should focus on combining the robust control theory with the generalized bias current linearization theory, thus making the MBCS able to cope with multiple operating conditions of the dynamic rotor.

REFERENCES

[1] M. Aenis, E. Knopf, and R. Nordmann, "Active magnetic bearings for the identification and fault diagnosis in turbomachinery," *Mechatronics*, vol. 12, no. 8, pp. 1011–1021, Oct. 2002.
[2] X. Tu, R. Zhou, Y. Zhou, and X. Cheng, "Dynamical decoupling and feedforward control for magnetically levitated planar actuators," *Int. J. Appl. Electromagn. Mech.*, vol. 54, no. 1, pp. 57–76, Apr. 2017.
[3] X. Tu, R. Zhou, Y. Zhou, X. Cheng, and C. J. T. Chien, "Measurement of initial phase for movers in magnetically levitated planar actuators," *Int. J. Appl. Electromagn. Mech.*, vol. 49, no. 1, pp. 91–104, Sep. 2015.
[4] Y. Zhu, S. Zhang, H. Mu, K. Yang, and W. Yin, "Augmentation of propulsion based on coil array commutation for magnetically levitated stage," *IEEE Trans. Magn.*, vol. 48, no. 1, pp. 31–37, Jan. 2012.
[5] X. Cheng, "Data interchange mechanism in multi-axis ultra-precise synchronous motion control system," *J. Mech. Eng.*, vol. 50, no. 17, pp. 149–156, 2014.
[6] C. Zhang, K. J. Tseng, T. D. Nguyen, and G. Zhao, "Stiffness analysis and levitation force control of active magnetic bearing for a partially-self-bearing flywheel system," *Int. J. Appl. Electromagn. Mech.*, vol. 36, no. 3, pp. 229–242, Jun. 2011.
[7] E. H. Maslen and G. Schweitzer, "Dynamics and control issues for fault tolerance," in *Magnetic Bearings Theory, Design, and Application to Rotating Machinery*. Berlin, Germany: Springer-Verlag, 2009, pp. 407–433.
[8] F. Gu, T. Wang, A. Alwodai, X. Tian, Y. Shao, and A. D. Ball, "A new method of accurate broken rotor bar diagnosis based on modulation signal bispectrum analysis of motor current signals," *Mech. Syst. Signal Process.*, vols. 50–51, pp. 400–413, Jan. 2015.
[9] X. Cheng, Q. Chen, H. Zeng, X. Wang, and R. Zhou, "Reconfiguration rules for loosely-coupled redundant supporting structure in radial magnetic bearings," *Int. J. Appl. Electromagn. Mech.*, vol. 51, no. 2, pp. 91–106, Jun. 2016.
[10] P. Schroder, A. J. Chipperfield, P. J. Fleming, and N. Grum, "Fault tolerant control of active magnetic bearings," presented at the IEEE Int. Symp. Ind. Electron. (ISIE), 1998, pp. 573–578.
[11] X. Cheng, H. Liu, S. Song, Y. Hu, B. Wang, and Y. Li, "Reconfiguration of tightly-coupled redundant supporting structure in active magnetic bearings under the failures of electromagnetic actuators," *Int. J. Appl. Electromagn. Mech.*, vol. 54, no. 3, pp. 421–432, Jul. 2017.
[12] E. H. Maslen and D. C. Meeker, "Fault tolerance of magnetic bearings by generalized bias current linearization," *IEEE Trans. Magn.*, vol. 31, no. 3, pp. 2304–2314, May 1995.
[13] U. J. Na and A. Palazzolo, "Optimized realization of fault-tolerant heteropolar magnetic bearings," *J. Vib. Acoust.*, vol. 122, no. 3, pp. 209–221, Jul. 2000.
[14] U. J. Na, A. B. Palazzolo, and A. Provenza, "Test and theory correlation study for a flexible rotor on fault-tolerant magnetic bearings," *J. Vib. Acoust.*, vol. 124, no. 3, pp. 359–366, Jul. 2002.
[15] M. D. Noh, S.-R. Cho, J.-H. Kyung, S.-K. Ro, and J.-K. Park, "Design and implementation of a fault-tolerant magnetic bearing system for turbomolecular vacuum pump," *IEEE/ASME Trans. Mechatronics*, vol. 10, no. 6, pp. 626–631, Dec. 2005.

[16] D. Meeker, "A generalized unbiased control strategy for radial magnetic bearings," *Actuators*, vol. 6, no. 1, p. 1, Jan. 2017.
[17] D. Montie and E. Maslen, "Self-sensing in fault tolerant magnetic bearings," *Trans. ASME*, vol. 123, no. 4, pp. 864–869, 2001.
[18] M. O. T. Cole, P. S. Keogh, M. N. Sahinkaya, and C. R. Burrows, "Towards fault-tolerant active control of rotor–magnetic bearing systems," *Control Eng. Pract.*, vol. 12, no. 4, pp. 491–501, Apr. 2004.
[19] L. M. A. Caseiro and A. M. S. Mendes, "Real-time IGBT open-circuit fault diagnosis in three-level Neutral-Point-Clamped voltage-source rectifiers based on instant voltage error," *IEEE Trans. Ind. Electron.*, vol. 62, no. 3, pp. 1669–1678, Mar. 2015.
[20] R. S. Srinivas, R. Tiwari, and C. Kannababu, "Model based analysis and identification of multiple fault parameters in coupled rotor systems with offset discs in the presence of angular misalignment and integrated with an active magnetic bearing," *J. Sound Vib.*, vol. 450, pp. 109–410, Jun. 2019.
[21] Z. Chilengue, J. A. Dente, and P. J. C. Branco, "An artificial immune system approach for fault detection in the stator and rotor circuits of induction machines," *Electr. Power Syst. Res.*, vol. 81, no. 1, pp. 158–169, Jan. 2011.
[22] W. Zhou, B. Lu, T. G. Habetler, and R. G. Harley, "Incipient bearing fault detection via motor current noise cancellation using Wiener filter," *IEEE Trans. Ind. Appl.*, vol. 45, no. 4, pp. 1309–1317, Jun. 2009.
[23] B. Li, P.-L. Zhang, Z.-J. Wang, S.-S. Mi, and D.-S. Liu, "A weighted multi-scale morphological gradient filter for rolling element bearing fault detection," *ISA Trans.*, vol. 50, no. 4, pp. 599–608, Oct. 2011.
[24] L. Saidi, F. Fnaiech, H. Henao, G.-A. Capolino, and G. Cirrincione, "Diagnosis of broken-bars fault in induction machines using higher order spectral analysis," *ISA Trans.*, vol. 52, no. 1, pp. 140–148, Jan. 2013.
[25] A. Bouzida, O. Touhami, R. Ibtiouen, A. Belouchrani, M. Fadel, and A. Rezzoug, "Fault diagnosis in industrial induction machines through discrete wavelet transform," *IEEE Trans. Ind. Electron.*, vol. 58, no. 9, pp. 4385–4395, Sep. 2011.
[26] I. S. Cade, P. S. Keogh, and M. N. Sahinkaya, "Fault identification in Rotor/Magnetic bearing systems using discrete time wavelet coefficients," *IEEE/ASME Trans. Mechatronics*, vol. 10, no. 6, pp. 648–657, Dec. 2005.
[27] L. Nagel, R. Galeazzi, A. J. Voigt, and I. F. Santos, "Fault diagnosis of active magnetic bearings based on Gaussian GLRT detector," presented at the 3rd Conf. Control Fault-Tolerant Syst. (SysTol), Sep. 2016, pp. 540–547.
[28] H. Shahnazari and P. Mhaskar, "Actuator and sensor fault detection and isolation for nonlinear systems subject to uncertainty," *Int. J. Robust Nonlinear Control*, vol. 28, no. 6, pp. 1996–2013, Apr. 2018.
[29] X. Cheng, B. Wang, Q. Chen, L. Zhang, H. Liu, and S. Song, "A unified design and the current ripple characteristic analysis of digital switching power amplifier in active magnetic-levitated bearings," *Int. J. Appl. Electromagn. Mech.*, vol. 55, no. 3, pp. 391–407, Oct. 2017.
[30] X. Cheng, L. Zhang, R. Zhou, S. Song, B. Wang, and H. Liu, "Analysis of output precision characteristics of digital switching power amplifier in the active magnetic bearings system," *Automatika*, vol. 58, no. 2, pp. 205–215, Apr. 2017.
[31] X. Cheng, B. Cheng, M. Lu, R. Zhou, and L. Zhang, "An online fault-diagnosis of electromagnetic actuator based on variation characteristics of load current," *Automatika*, vol. 61, no. 1, pp. 11–20, Jan. 2020.

XIN CHENG was born in Wuhan, China, in October 1982. He received the B.S. degree in information engineering and the M.S. degree in communication and information system from the Wuhan University of Technology, Wuhan, in 2004 and 2007, respectively, and the Ph.D. degree in mechanical and electronic engineering from the Huazhong University of Technology, Wuhan, in 2011.

He is currently an Associate Professor with the School of Mechanical and Electronic Engineering, Wuhan University of Technology. His research interests include motion control, magnetic bearings, and advanced servo systems.

SHUAI DENG was born in Xinxiang, China, in 1991. He is currently pursuing the Ph.D. degree with the School of Mechanical and Electronic Engineering, Wuhan University of Technology. His research interests include magnetic bearings and dynamics of rotating machines.

BAI-XIN CHENG was born in Liaocheng, China, in 1990. He is currently pursuing the Ph.D. degree with the School of Mechanical and Electronic Engineering, Wuhan University of Technology. His research interests include magnetic bearings and dynamics of rotating machines.

YE-FA HU was born in December 1961. He received the Ph.D. degree in mechanical and electronic engineering from the Wuhan University of Technology, Wuhan, China, in 2001. He is currently a Full Professor with the School of Mechanical and Electronic Engineering, Wuhan University of Technology. His research interests include magnetic levitation technology, mechatronics, and digital manufacturing.

HUA-CHUN WU was born in November 1976. He received the Ph.D. degree in mechanical and electronic engineering from the Wuhan University of Technology, Wuhan, China, in 2005. He is currently a Full Professor with the School of Mechanical and Electronic Engineering, Wuhan University of Technology. His research interests include magnetic bearing technology, device state monitoring and fault diagnosis, and artificial heart pump.

ROU-GANG ZHOU (Member, IEEE) was born in Taizhou, Zhejiang, in 1984. He received the Ph.D. degree in mechanical and electronic engineering from the Huazhong University of Science and Technology, in 2015. He is currently a Full Professor and a Master-Studies Supervisor with the College of Mechanical Engineering, Hangzhou Dianzi University. His research interests include precision motion control, maglev planar motor, and machine vision.